Path Integral Studies of the Rotations of Methane and Its Heavier Isotopomers in ^{4}He Nanoclusters

N. D. Markovskiy and C. H. Mak*

Department of Chemistry, University of Southern California, Los Angeles, California 90089-0482

Received: January 23, 2009; Revised Manuscript Received: June 20, 2009

Path integral Monte Carlo simulations have been carried out to study the rotations of a methane molecule and its heavier isotopomers inside a small cluster of ^{4}He atoms at 0.3 K in order to determine how the renormalization in the methane's rotational constant is related to the quantum statistics and superfluidity of the helium shell. By changing the mass of the hydrogens and systematically varying the moment of inertia of the methane, we were able to study the effects of its rotations on the quantum statistics of the helium atoms and their countereffects on the methane's effective rotational constant. The renormalized rotational constant depends strongly on the intrinsic moment of inertia of the methane. A heavy probe favors strong templating of the helium density as well as a large renormalization in the probe's rotational constant, but a light probe shows almost no effect on the shell density or the effective rotational constant. These results suggest that in order to fully understand the superfluidity of the helium shell, the probe must be treated as an integral part of the system. We rationalize the findings in terms of a rotational smearing effect and suggest that there is no clearly quantifiable relationship between the superfluid fraction of the shell and the renormalized rotational constant of the probe for cases where the probe molecule is either light or has weak anisotropic interactions with the helium atoms.

I. Introduction

The discovery of superfluidity in liquid ^{4}He has attracted the interest of many. Early theoretical work, neutron scattering experiments, and, more recently, quantum simulations have greatly facilitated the understanding of superfluid behavior in the bulk.[1,2] The peculiar properties of superfluid ^{4}He are largely captured by the two fluid theory of Tisza and Landau.[3−5] In this picture, the superfluid fraction is defined by the nonclassical response of the fluid to a slowly rotating macroscopic probe.

More recently, a molecular version of the rotating disk experiment of Andronikashvili[6] has been carried out using ^{4}He nanodroplets.[7] In these experiments, the effects of the helium atoms on a rotating molecular probe embedded inside the droplet was measured spectroscopically. The earliest experiments were carried out using heavy probe molecules, like SF_6 and OCS.[7,8] The observations of sharp rotational features in helium nanoclusters were explained using ideas borrowed from bulk superfluidity.[9] In general, the effective rotational constants of these heavy probes inside helium droplets are modified by a factor of about 3−5 from their gas-phase values. These experiments have also been performed more recently employing lighter probes, such as NH_3, HF, CH_4, and C_2H_2.[10−15] These revealed much smaller renormalizations in the probe's effective rotational constants, from being nearly identical to their gas-phase values for very light probes to 3−4 for probes of intermediate to heavy masses. The experimentally observed renormalization in the rotational constants therefore seems to be strongly dependent on the specific nature of the probes themselves. Recent experiments with much smaller helium clusters[16−19] suggest that very similar effects are observable with a single shell or even a partial shell of ^{4}He atoms.

An important question presented by these experiments is whether there exists a universal relationship between the observed renormalized rotational constant and the nonclassical superfluid response of the ^{4}He shell. To fully address this, experimental and theoretical studies must be carried out on a variety of different probe molecules to look for systematic trends. On the theoretical front, the quantum mechanics of the probe rotations must be incorporated into the calculations in a rigorous manner. Most of the calculations that explicitly address the interaction between rotations of the probe and the ^{4}He have been carried out for linear molecules.[19−30] So far, rotors of other symmetries have not been studied extensively. For spherical top molecules, only one theoretical calculation has been published explicitly addressing the rotations of SF_6 in ^{4}He using zero-temperature diffusion Monte Carlo.[9,31,32] Interestingly, a recent numerical study[33] suggests that the anisotropy and the strength of the ^{4}He−probe interactions may be more important for determining the rotational constant renormalization than the intrinsic moment of inertia of the probe, but only linear molecules were examined. Also, a comprehensive study of the effects of the rotations of probes of different symmetries on the helium densities have been reported based on a diffusion Monte Carlo calculation,[34] but being a zero-temperature study, it also provides no direct information on the relationship between the renormalized rotational constant and the superfluidity of the helium shell.

In this paper, we report a finite-temperature path integral Monte Carlo (PIMC) study of another spherical top molecule, methane, and its heavier isotopomers. Our main focus is to examine the effects of the mass and the intrinsic moment of inertia of the methane on the quantum statistics of the ^{4}He atoms and their influence on the observed renormalization in the methane's rotational constant. This was carried out in the simulations by systematically varying the hydrogen atoms mass. The paper is organized as follows. In section II, we briefly review the path integral method and give a computationally efficient treatment of the rotations of spherical top molecules. After the theoretical background, we discuss the implementation

10.1021/jp900718d CCC: $40.75 © 2009 American Chemical Society
Published on Web 07/20/2009

of a multilevel approach for simulating the path integrals. In section III, we explain the methodology of extracting rotational constants from imaginary-time orientation correlation function and provide several examples. Starting with a "heavy" methane with a moment of inertia 50 times larger than normal CH_4, we measured the effective rotational constants and the corresponding angular helium density profiles with and without exchange. Then the moment of inertia of the methane was gradually increased to search for systematic variations in the probe's rotational constant. The observed effects are discussed and rationalized by a simple model in section IV.

II. Theory and Numerical Implementation

A. Path Integral. The equilibrium statistics of a quantum system within the canonical ensemble can be represented by path integrals. In the path integral picture, the density matrix operator $\hat{\rho} = \exp(-\beta\hat{H})$ is first written as a product of n high-temperature propagators using the Trotter product formula[35]

$$\hat{\rho} = [e^{-\tau\hat{H}}]^n$$

where $\beta = 1/k_B T$, T is the temperature, $\hat{H}$ is the Hamiltonian, and $\tau = \beta/n$. In analogy to real-time path integrals, β is often called the "imaginary-time", and the high-temperature propagators are thus referred to as the "short-time" propagators.

When the system has both translational and rotational degrees of freedom, the path-integral form of the density matrix becomes

$$\hat{\rho}(\beta, \mathbf{R}, \mathbf{R}') = \int \hat{\rho}(\tau, \mathbf{R}, \mathbf{R}_1)\cdots\hat{\rho}(\tau, \mathbf{R}_n, \mathbf{R}')\, d\mathbf{R}_1\cdots d\mathbf{R}_n \quad (1)$$

where vectors $\mathbf{R}_i$ consist of rotational, $\mathbf{\Omega}_i$, and translational, $\mathbf{r}_i$, degrees of freedom and $\rho(\tau,\mathbf{R}_i,\mathbf{R}_{i+1})$ are short-time propagators of the system. In the absence of interactions, eq 1 is exact for any n. But when interactions are included, the short-time propagators must be first approximated by a "short-time approximation" ρ and the path integral is written as the limit

$$\hat{\rho}(\beta, \mathbf{R}, \mathbf{R}') = \lim_{n\to\infty} \int \rho(\tau, \mathbf{R}, \mathbf{R}_1)\cdots\rho(\tau, \mathbf{R}_n, \mathbf{R}')\, d\mathbf{R}_1\cdots d\mathbf{R}_n \quad (2)$$

In order for eq 2 to converge to the original density matrix, the short-time approximation $\rho(\tau,\mathbf{R},\mathbf{R}')$ must be correct to first order in τ. One commonly used approximation is the "primitive" discretization[2]

$$\rho(\tau, \mathbf{R}_i, \mathbf{R}_{i+1}) = \hat{\rho}^{\mathrm{rot}}(\tau, \mathbf{\Omega}_i, \mathbf{\Omega}_{i+1})\hat{\rho}^{\mathrm{trans}}(\tau, \mathbf{r}_i, \mathbf{r}_{i+1}) \times e^{-\tau/2[V(\mathbf{R}_i)+V(\mathbf{R}_{i+1})]} \quad (3)$$

where V is the potential and $\hat{\rho}^{\mathrm{rot}}$ and $\hat{\rho}^{\mathrm{trans}}$ are the *exact* rotational and translational propagators of the free system. The translational propagators in eq 3 for the center-of-mass motions can be written in the usual form[2]

$$\hat{\rho}(\tau, \mathbf{r}_i, \mathbf{r}_{i+1}) = \left(\frac{m}{2\beta\pi\hbar^2}\right)^{1/2} \exp\left[-\frac{m}{2\beta\hbar^2}|\mathbf{r}_i - \mathbf{r}_{i+1}|^2\right]$$

where m is the mass. On the other hand, the rotational propagator takes the form[36]

$$\rho^{\mathrm{rot}}(\tau, \mathbf{\Omega}, \mathbf{\Omega}') = \sum_{j,k,m} e^{-\tau E_k^{jm}} \langle\Omega|jkm\rangle\langle jkm|\Omega'\rangle \quad (4)$$

where $\langle\mathbf{\Omega}|jkm\rangle$ are asymmetric top wave functions, which can be expressed in the basis of eigenvectors of a symmetric top molecule $[(2j+1)/8\pi^2]^{1/2}D_{k,m}^{j}(\phi,\theta,\chi)$, and $D_{k,m}^{j}(\phi,\theta,\chi)$ are Wigner's functions and ϕ, θ, and χ are the Euler angles.[37] For a spherical top molecule, such as CH_4, the full rotational propagator in eq 4 reduces to the standard form

$$\rho^{\mathrm{rot}}(\tau, \mathbf{\Omega}, \mathbf{\Omega}') = \frac{1}{8\pi^2}\sum_{j,k,m}(2j+1)e^{-\tau Bj(j+1)}D_{k,m}^{\ j}(\phi,\theta,\chi) \times D_{k,m}^{\ j^*}(\phi',\theta',\chi') \quad (5)$$

The three Euler angles can more conveniently be parametrized as the angles describing points on a unit sphere embedded in four dimensions, taking the forms[38]

$$\begin{aligned} e_0 &= \cos\frac{\theta}{2}\cos\frac{\phi+\chi}{2} \\ e_1 &= \sin\frac{\theta}{2}\sin\frac{\phi-\chi}{2} \\ e_2 &= \sin\frac{\theta}{2}\cos\frac{\phi-\chi}{2} \\ e_3 &= \cos\frac{\theta}{2}\sin\frac{\phi+\chi}{2} \end{aligned} \quad (6)$$

such that $e_0^2 + e_1^2 + e_2^2 + e_3^2 = 1$. The rotational path integrals can therefore be more conveniently represented as trajectories on the surface of a four-dimensional hypersphere, spanned by these vectors. As in the case of spherical harmonics, a sum rule exists for the hyperspherical harmonics, leading to the Chebyshev polynomials of the second kind[39]

$$\sum_{k,m} D_{k,m}^{\ j}(\mathbf{\Omega})D_{k,m}^{\ j^*}(\mathbf{\Omega}') = U_{(2j)}(\mathbf{e}\cdot\mathbf{e}')$$

In terms of the Chebyshev polynomials, the rotational propagator can finally be written as[39−42]

$$\hat{\rho}^{\mathrm{rot}}(\tau, \mathbf{\Omega}, \mathbf{\Omega}') = \sum_j \frac{(2j+1)}{8\pi^2} e^{-\tau Bj(j+1)} U_{(2j)}(\mathbf{e}\cdot\mathbf{e}') \quad (7)$$

This form allows for efficient computation of the rotational density matrix during the path-integral simulations.

For interacting systems with a nonzero potential V, the propagator can be approximated by the primitive discretization in eq 3 above. This primitive approximation is straightforward to implement in a path integral simulation, but a large n is often required for convergence. This in turn leads to slow sampling problems which are often encountered in path integral simulations.[43] As mentioned above, any approximate propagator correct to first order in $\tau = \beta/n$ will generate the exact density matrix in the limit $n \to \infty$. Therefore, it is also possible to use alternative approximations which are more accurate and require fewer discretizations n to converge. This approach was taken by Ceperley et al. in a number of previous path integral simulations

of low-temperature helium,[1] where a "two-particle density matrix approximation" was used to keep n small. This approximately accounts for the effect of the pair interaction potential by using the two-particle propagator as the basis for the Trotter breakup, and it accelerates the convergence considerably so that a much smaller n may be used in the simulation. But this is also more difficult to implement for anisotropic systems due to operating memory constraints.

For problems with rotational degrees of freedom, the primitive approach is preferred in order to simplify the inclusion of rotational motions into the path integral simulations. But if one chooses to use the primitive approach, more elaborate Monte Carlo moves must be incorporated in order to overcome the typical slow sampling problems. A possible approach was given by Mak and Zakharov.[43] This method uses multilevel moves to update the paths, allowing nonlocal changes to the paths. This approach has been implemented for the translational degrees of freedom in a simulation of bosonic *para*-hydrogen[44] but not yet for rotational paths.

B. Multilevel Algorithm for Rotations. As mentioned above, the rotational paths can be represented by trajectories on the surface of a four-dimensional unit sphere. In imaginary time, these paths are closed; i.e., the beginning and end points of a path must coincide due to the trace operation inherent in the partition function. The objective of the multilevel algorithm is to find ways to sample these closed paths efficiently.

The most straightforward way to carry out Monte Carlo sampling is probably the Metropolis method.[45] When applied to rotational path sampling, the Metropolis algorithm would sample a new set of the three Euler angles ϕ_i, θ_i, and χ_i on time slice i from the Jacobian $\mathrm{d}\Omega = \mathrm{d}\phi\,\mathrm{d}\chi\,\mathrm{d}\cos\theta$ and accept or reject them based on the acceptance probability

$$P = \min[1, \rho(\tau, \mathbf{R}_i^{\text{new}}, \mathbf{R}_{i+1}^{\text{new}})/\rho(\tau, \mathbf{R}_i^{\text{old}}, \mathbf{R}_{i+1}^{\text{old}})]$$

where ρ is the short-time propagator in the primitive discretization from eq 3. In order to obtain converged results, the primitive discretization requires a large n and hence a small τ. In this limit, the rotational propagator is sharply peaked at small displacements $\delta R = \mathbf{R}_{i+1} - \mathbf{R}_{i+1}$ causing extremely narrow rotational dispersion in a single time slice. This in turn leads to slow sampling problems when the Metropolis algorithm is used to simulate path integrals.

The slow sampling problem may be cured if one is able to generate large sections of the rotational path spanning several time slices at a time. This is because longer-time path segments are more delocalized in space and sampling them will reduce the correlation between the samples. But to do this, we will need additional knowledge about the distribution in question. We will now outline a procedure that can be used to generate long-time rotational paths efficiently.

The objective is to sample long-time paths parametrized by the set of discrete points ($\mathbf{R}_1$, $\mathbf{R}_2$, $\cdots$ $\mathbf{R}_{N-1}$) with fixed end points $\mathbf{R}_0$, $\mathbf{R}_N$ and imaginary time $t = N\tau$ from the distribution $\prod_{i=0}^{N-1}\rho(\tau,\mathbf{R}_i,\mathbf{R}_{i+1})$. We take $N = 2^M$, and refer to M as the number of "levels" in calculation. One starts at the top level $m = M$, where the path consists the entire time slice t with the two points $\mathbf{R}_0$ and $\mathbf{R}_F$. At the next lower level $m = M - 1$, the path is bisected in time and the midpoint $\mathbf{R}_{N/2}$ is sampled from the conditional probability distribution with the finer levels integrated out

$$\Pi\left(\mathbf{R}_{N/2}, \frac{t}{2}\middle|\mathbf{R}_0, \mathbf{R}_F\right) = \frac{\rho(\mathbf{R}_0, \mathbf{R}_{N/2}, t/2)\rho(\mathbf{R}_{N/2}, \mathbf{R}_F, t/2)}{\rho(\mathbf{R}_0, \mathbf{R}_F, t)} \tag{8}$$

where $\rho(\mathbf{R}_0,\mathbf{R}_F,t)$ provides the proper normalization. At level $m = M - 2$ with time slice $t/4$, we sample two more points, conditional to the end points and the midpoint $\mathbf{R}_{N/2}$ from the previous level. In other words, one applies the exact same procedure as in the previous level (level $M - 1$) to the end points $\mathbf{R}_0$, $\mathbf{R}_{N/2}$ to sample $\mathbf{R}_{N/4}$, and $\mathbf{R}_{N/2}$, $\mathbf{R}_F$ to get $\mathbf{R}_{3N/4}$. The procedure can then be repeated recursively down to level $m = 0$ until the whole path is constructed. The only requirement is that the exact analytical expression for the conditional distribution

$$\int \rho(\mathbf{R}_i, \mathbf{R}, \tau/2)\rho(\mathbf{R}, \mathbf{R}_{i+1}, \tau/2)\,\mathrm{d}\mathbf{R} = \rho(\mathbf{R}_i, \mathbf{R}_{i+1}, \tau)$$

is known for arbitrary time scale up to time t. For a free particle or a rigid free rotor, this is no problem. The method of bisecting the free-particle path with respect to the translational degrees of freedom is the basis of the bisection algorithm described by Ceperley in ref 1 and the multilevel path sampling algorithm of Mak et al.[43] With respect to rotations, the challenge comes from the fact that the conditional probabilities eq 8 do not have the free particles Gaussian nature and the corresponding cumulative probabilities

$$\rho(\phi, \theta, \chi; \mathbf{\Omega}_i, \mathbf{\Omega}_{i+1}, \tau) = \rho(\mathbf{\Omega}_i, \mathbf{\Omega}, \tau)\rho(\mathbf{\Omega}, \mathbf{\Omega}_{i+1}, \tau)$$

need to be integrated numerically. In order to do that, we have implemented a numerical procedure based on the rejection method. The distribution is approximated by its covering piecewise constant function $f(\phi,\theta,\chi;\mathbf{\Omega}_i,\mathbf{\Omega}_{i+1},\tau)$ and ϕ, θ, and χ are put on an adaptive grid such that $f(\phi,\theta,\chi;\mathbf{\Omega}_i,\mathbf{\Omega}_{i+1},\tau)$ covers the original function and the points are concentrated around its peak. Moreover, one also needs an additional grid containing the final positions $\mathbf{\Omega'}_{i+1}$, $\mathbf{\Omega}_{i+1}$ in the frame of initial positions $\mathbf{\Omega}_i$ for each imaginary time level. With that, the conditional cumulative probabilities $f^c(\phi;\tau,\mathbf{0},\mathbf{\Omega'}_{i+1})$, $f^c(\theta;\tau,\mathbf{0},\mathbf{\Omega'}_{i+1}|\phi)$, and $f^c(\chi;\tau,\mathbf{0},\mathbf{\Omega'}_{i+1}|\theta,\phi)$ can be precomputed and stored in advance. During the simulation, ϕ, θ, and χ are sampled from the approximate rigid spherical top distribution by the rejection method. This allows one to generate a long time free rotor path between two arbitrary end points. After the path is constructed, it is finally accepted based on the total potential in the Metropolis fashion.

III. Results

Normal CH_4 is a rather light rotor with a gas-phase rotational constant $B = 5.24\ \mathrm{cm}^{-1}$.[46] Experiments on normal and deuterated methane rotations in ^{4}He droplets had been performed,[13,14,47] both showing very weak renormalization in B. Heavier isotopomers of methane are of course experimentally inaccessible. The advantage of theory is that we can vary the moment of inertia of the CH_4 molecule while holding everything else fixed, allowing us to isolate the effects of the rotor's moment of inertia and examine its influence on the rest of the properties of the system. In our simulations, we measured the superfluid response and the renormalization of the B constant for a variety of probe moments of inertia, from 1 time to 50 times normal methane. In the rest of this paper, we will simply denote these methane isotopomers by their hydrogen mass, e.g., $2 \times CH_4$ would correspond to deuterated methane. Since the main purpose of this study is to investigate the systematic effects of the probe's

moment of inertia on the ^{4}He shell but not on normal methane specifically, we have intentionally left the hydrogen atom nuclear spin out of the rotational path integrals of the methane. In a future study, we will re-examine normal methane rotations in greater detail with the full inclusion of proper nuclear spin statistics.

In each calculation reported here, a single methane with a certain hydrogen atom mass was simulated with a fixed number of ^{4}He atoms around it. The interactions between methane and heliums were modeled by the Buck potential[48] and the He−He interactions by the Aziz potential.[49] All simulations were carried out at a constant temperature of 0.3 K with an imaginary-time discretization of 1024 beads for both the translational and rotational degrees of freedom. Convergence was checked against larger discretizations. With $n = 1024$, the systematic error in the superfluid fraction was less than 1%. Approximately 12 He atoms are sufficient to complete the first solvation shell; consequently, most of the detailed calculations have been performed for this cluster size. For 12 ^{4}He and at 0.3 K, the total ^{4}He superfluid density is close to unity. In this study, we have focused on the properties of small $CH_4-(^4He)_N$ clusters ($N \leq 20$) only.

A. Effective Rotation Constants for Heavy Probes. According to the experiments, dynamical measurables like the rovibrational spectra of the probe embedded in ^{4}He clusters seem to suggest quantum statistics are important. Extracting dynamical properties from the simulations would entail either a real-time path integral calculation or an analytic continuation of imaginary-time correlation function data, both of which are notoriously difficult. In the recent works of Paesani et al.[50] and Moroni et al.,[26] maximum entropy analyses and multiexponential fits were applied to the orientation correlation function in order to extract the spectral features. Recently, an alternative method has been suggested by several groups to estimate the renormalized B constant using imaginary-time data alone based on the orientational correlation function of the probe.[20−22] Blinov et al.[22] suggested using the imaginary-time correlation function

$$\langle \hat{\mathbf{n}}(\tau)\cdot\hat{\mathbf{n}}(0)\rangle = \frac{1}{Z}Tr\{e^{-\beta\hat{H}}e^{\tau\hat{H}}\hat{\mathbf{n}}e^{-\tau\hat{H}}\hat{\mathbf{n}}\}$$

where $\hat{\mathbf{n}}$ is a unit vector describing the orientation of the molecule relative to the laboratory frame and $Z = \langle \hat{\mathbf{n}}(0)\cdot\hat{\mathbf{n}}(0)\rangle$. They fit this to the analytical expression for a rigid top molecule to extract an effective B constant, allowing them to estimate the renormalized rotational constant of the OCS molecule without real-time path integrals.[51] We have adopted a similar approach in our work. For our case, the probe and the average density have overall spherical symmetry; it is therefore logical to fit the simulation results to a rigid spherical top orientation correlation function, for which the following analytical expression can be derived straightforwardly

$$Z\langle \hat{\mathbf{n}}(\tau)\cdot\hat{\mathbf{n}}(0)\rangle = e^{-2B\tau} + \sum_{j>0}\left(\sum_{k\leq j-1}\frac{j^2-k^2}{j}e^{-\beta Bj(j+1)+2\tau Bj} + \sum_{k\leq j}e^{-\beta Bj(j+1)}\left[\frac{(2j+1)k^2}{j(j+1)} + \frac{(j+1)^2-k^2}{j+1}e^{-2\tau B(j+1)}\right]\right)$$

where B is the effective rotational constant of a spherical top molecule. Examples of the orientation correlation function are shown in Figure 1 for CH_4 ($B = 5.24$ cm^{-1}), $2 \times CH_4$ and $50 \times CH_4$ in the gas phase, as well as a $50 \times CH_4$ surrounded by 12 bosonic ^{4}He. Blinov et al.[22,30] reported that this fitting procedure is imperfect, especially for the linear rotors treated previously. However, Figures 1, 2, and 5 indicate that the quality of the fits for the CH_4−helium clusters is reasonably good. In the following figures, the error bars given for the B constants account for the imprecision of this fit.

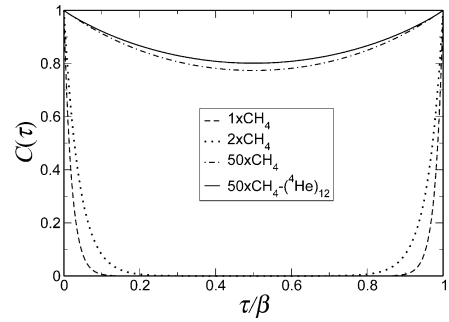

Figure 1. Examples of the orientation correlation function for normal CH_4, $2 \times CH_4$, and $50 \times CH_4$ in the gas phase, as well as $50 \times CH_4$ inside a shell of 12 ^{4}He atoms.

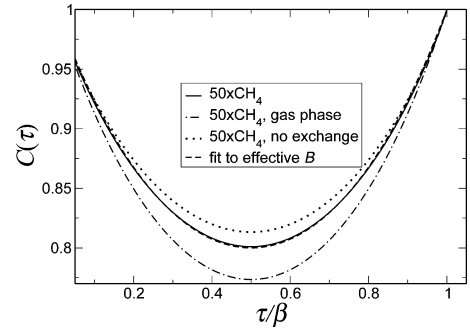

Figure 2. Orientation correlation function of $50 \times CH_4$ in a shell of 12 ^{4}He atoms (solid line) and the best fit to a rigid spherical top model (dashed line), compared to the nonexchange result (dotted line) and the gas phase (dotted dashed line).

We start by summarizing the results for the heaviest rotor we have studied, a $50 \times CH_4$. To extract the effective B constant for $50 \times CH_4$ embedded in 12 ^{4}He, we fit its correlation function to that of a free spherical top molecule. The fit is shown in Figure 2. The statistical error of the orientation correlation function is comparable to the width of the line in the plot. The fitted value corresponds to an effective B constant of 0.091 cm^{-1}, compared to 0.105 cm^{-1} for a $50 \times CH_4$ molecule in the gas phase.

To assess the effects of quantum statistics, we carried out the same simulation turning off all the exchanges among the helium atoms. The correlation function for this nonexchange case is shown in Figure 2 as the dotted line. The nonexchange correlation function lies above the exchange result, indicating that exchange facilitates more rotational freedom for the $50 \times CH_4$. The effective B constant in nonexchange helium is 0.086 cm^{-1}. Relative to the gas-phase value, the renormalized B constant for $50 \times CH_4$ is 13.3% and 15.6% smaller in ^{4}He, for the exchange and nonexchange cases, respectively. These correspond to an effective increase in the moment of inertia of the probe from 160.85 amu·Å^2 to 185.65 and 190.35 amu·Å^2 for the exchange and nonexchange cases, respectively. Overall, these results are qualitatively very similar to what was observed for linear rotors previously, showing that bosonic effects promote rotational freedom of a heavy rotor, though the magnitude of the B constant renormalization is much smaller in this case (13.3% here versus 177% in OCS[52]).

B. Effects of Probe Rotations on the Helium Shell. Next, we will proceed to results regarding the helium shell density and its superfluidity. Before we present them, it is important to point out that the prevailing notion of adiabatic following is based on the interaction (or more precisely the lack of it) between the superfluidity local to the molecule with the rotational motions of the probe through the anisotropic coupling between the probe and the shell. As such, there ought to be three key parameters in determining whether adiabatic following is in effect. These are (1) the local superfluid density, (2) the intrinsic rotational dynamics of the bare molecule, and (3) the strength of the anisotropic coupling between the molecule and the helium, which are not all independent of each other when it comes to real molecules. Therefore, to understand these effects separately, a theoretical calculation can systematically vary one or more of these three parameters without touching the rest. This will allow us to assess the importance of each factor independently. In this paper, we have kept the He−CH_4 interaction fixed but varied the other two parameters by tuning the intrinsic moment of inertia of the probe as well as turning the exchanges among the ^{4}He on or off. Furthermore, the incomplete shell results to be presented in section III.D give us another handle on the effects of the local superfluidity.

To measure the superfluid density, we followed the method given by Ceperley.[1] This recipe in principle only provides the global superfluid fraction, but since our study is limited to fewer than 20 heliums atoms, which barely completes the first solvation shell, the superfluid density local to the molecule should be almost entirely identical to the global superfluid density, especially for the smallest clusters considered. Furthermore, the high symmetry of the CH_4 molecule and the weak anisotropy of the He−CH_4 interaction make this even more so for CH_4 than for other (mostly linear) probes studied before. Finally, as we will see below, the superfluid fraction for the clusters in the size range between 6 and 20 heliums are all larger than 0.85, which almost guarantees that the local superfluid densities are either identical or very close to the global superfluid densities. To be sure, we have computed the local superfluid densities according to two different prescriptions given by Whaley et al.,[9,20,53−57] using (a) a local decomposition of the global superfluid density from the projected areas of the paths and (b) an exchange-length-based local estimate of the nonsuperfluid densities. As is well-known,[55] method (a) is applicable to nonrotating molecules or heavy probes where the global superfluid density can be decomposed into local contributions inside the rotating frame of the molecule. For light molecules, method (b) is more appropriate, but there is no definitive criterion for deciding what is the minimum length of the permutation cycle for a path to be considered part of the superfluid densities. Despite the issues with both methods, we computed both quantities and compared them to the global superfluid densities. As expected, both of these quantities are imperfect, but they produce results almost identical to the global superfluid density, especially for cluster sizes below the first solvation shell, giving us confidence that the results are consistent. In the following, we will report the global superfluid densities in most cases. In situations where the local superfluid densities are important, we will report results using method (a) integrated over all angles and up to a certain radial distance from the CH_4.

Figure 3a shows the angular density of the He atoms in a $50 \times CH_4-(He)_{12}$ cluster on the surface of the probe molecule, integrated over all distances in the radial direction, on a false color scale. All of the 12 heliums are completely in the first solvation shell. The picture reveals four regions of low densities, with one of the four hydrogen atoms of the methane positioned at the center of each. The rest of the helium density is characterized by interconnecting higher-density channels on the surface of the CH_4. Figure 3a shows that there are 10 density maxima inside the channels and 4 weaker local maxima centered on the hydrogen atoms. The helium atoms sample the potential surface and assemble into a close-packed-like structure, indicating strong templating effects by the probe molecule underneath. The helium density variation from minimum to maximum in Figure 3a is approximately a factor of 2 for $50 \times CH_4-(He)_{12}$. We have also studied the shell density in the nonexchange case where all exchanges were turned off and found essentially no difference in the helium density between the exchange and nonexchange cases.

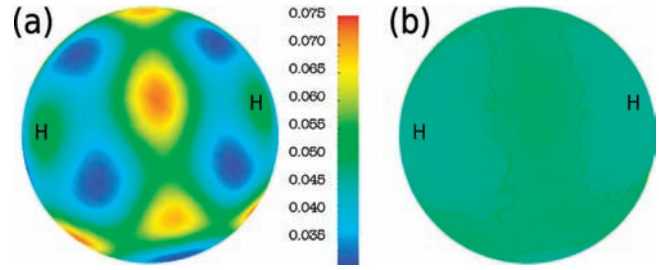

Figure 3. Angular density profile of the ^{4}He shell in a (a) $50 \times CH_4-(He)_{12}$ and (b) $1 \times CH_4-(He)_{12}$ cluster. H shows the positions of the hydrogen atoms. The ^{4}He density is strongly templated by the heavy probe, while it is almost completely isotropic for the light probe.

Previous studies on SF_6 in ^{4}He droplets found similar templating effects of the probe on the helium atoms in the first solvation shell.[9] On the basis of those results, a microscopic two-fluid model was proposed to rationalize the superfluid response of the helium atoms. It would therefore be interesting to examine whether this templating effect is reflected in the superfluid density of the shell in the case of CH_4 too. We measured the superfluidity of the ^{4}He by the standard method of Ceperley.[1] For $50 \times CH_4-(He)_{12}$, the superfluid fraction of the shell turns out to be surprisingly large. The simulations show a $96 \pm 1\%$ superfluid fraction, despite the heavy templating by the probe. Even though there is a distinct closed-packed-like structure in the helium density, the exchanges can apparently occur quite efficiently along the interconnected higher-density channels on the surface of the CH_4 molecule, encompassing almost the entire shell. Thus, the ability of the helium atoms to undergo exchange must be related to the density modulations in the helium shell, which are in turn dictated by the anisotropy of the interactions between the probe and the ^{4}He atoms, as well as by the intrinsic moment of inertia of the probe.

If we assume the nonsuperfluid fraction of the helium shell follows the rotation of the probe adiabatically, one can estimate the resulting change in the moment of inertia of the probe. On the basis of a 4% nonsuperfluid fraction and an average separation of approximately 4.05 Å between the helium atoms and the probe, the effective moment of inertia of the rotor is expected to increase by 13%, assuming the nonsuperfluid fractions are uniformly distributed on the shell. On first sight, this estimate appears to be in good agreement with the renormalization in the observed B constant in Figure 2 for the exchange case, which is 13.3%. But if one applies the same logic to the nonexchange case where 100% of the shell is nonsuperfluid, then one would have expected a 2500% renormalization in the B constant. Figure 2 shows only a 20%

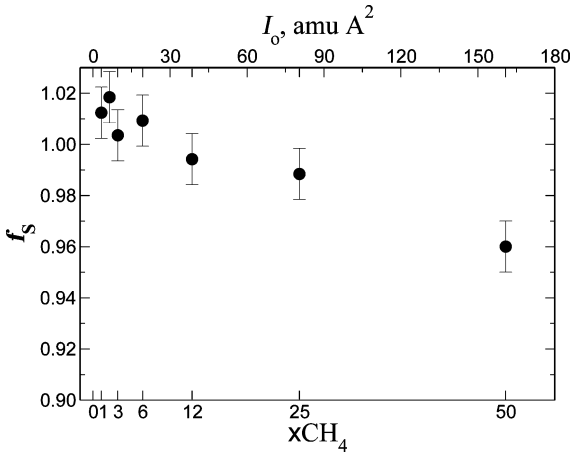

Figure 4. The superfluid fraction of the helium shell for 50 × to 1 × CH_4 with 12 ^{4}He atoms.

renormalization for the nonexchange case; therefore, while the renormalized *B* constant appears to be consistent with the amount of nonsuperfluid helium atoms in the exchange case, this agreement must be taken to be fortuitous and the concept of adiabatic following in the case of CH_4 where the anisotropic interaction between the methane and the shell is weak does not seem to apply. The data to be presented in section III.D will further corroborate this point.

Next, we turn to the results for the lighter probes. Figure 3b shows angular ^{4}He density for a 1 × CH_4. In comparison to 50 × CH_4, the ^{4}He density is now almost uniform over the entire shell with a minimum-to-maximum variation of only 7%. This suggests that the rotational dispersions of a light probe lead to almost no templating of the helium density, in sharp contrast with what was observed for 50 × CH_4. For all practical purposes the helium atoms seem to be distributed uniformly around the 1 × CH_4. This of course does *not* imply that there is no internal structure in the helium shell itself. The helium atoms have repulsive interactions and must pack around the methane to avoid steric overlap with other helium atoms. But the overall packing seems to be insensitive to the orientation of the underlying 1 × CH_4. Since methane is light, it also has substantial translational quantum dispersion. To rule out the possibility that the translational dispersion may be responsible for the weak templating, we have performed a simulation for 1 × CH_4 with all its rotations turned off. With translational dispersion only, the ^{4}He shell density reverted to strong modulations similar to those observed for 50 × CH_4 in Figure 3a. Therefore, the shell density differences between 50 × CH_4 and 1 × CH_4 seen in Figure 3 must be primarily due to rotational effects.

Figure 4 shows how the superfluid fraction varies with the intrinsic moment of inertia of the probe, from 50 × all the way to 1 × CH_4. Starting at 96% for 50 × CH_4, the superfluid fraction increases quickly to 100% when the intrinsic moment of inertia of CH_4 is decreased. The reason for this increase in the superfluid fraction for lighter probes is related to the helium shell density. The extremely weak templating by the lighter probes enables rapid exchanges among the ^{4}He atoms on the shell, leading to a superfluid fraction close to unity.

C. Effective Rotation Constants for Light Probes. Figure 5 shows the orientation correlation function for the 1 × CH_4 in 12 ^{4}He atoms with full exchange, compared to the free CH_4 molecule in the gas phase. The fit to a free rotor orientation correlation function yields a renormalized *B* constant of about 5.10 cm^{-1}. This corresponds to an effective increase in the

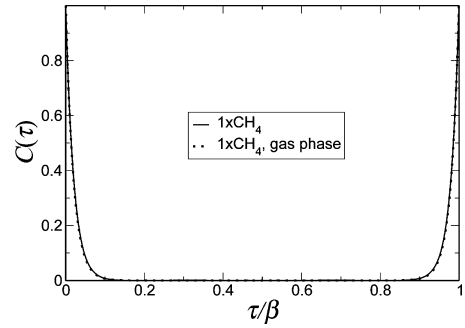

Figure 5. Orientation correlation function of 1 × CH_4 in a shell of 12 ^{4}He atoms (solid line) compared to the gas phase (dotted line).

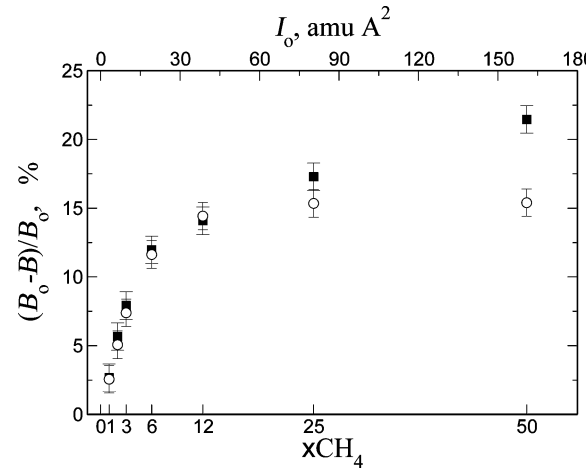

Figure 6. The percentage change in the effective *B* constant as a function of the intrinsic moment of inertia of the probe with full exchange (circles) and no exchange (squares).

moment of inertia of the probe from 3.217 amu·Å^2 in the gas phase to 3.30 amu·Å^2 in helium, a mere 3% change. This result is unaltered whether exchanges are turned on or off. This suggests that the lack of rotational slowing in the case of a light CH_4 bears no direct relationship with the superfluidity of the shell—the molecule has the same effective *B* constant with or without exchanges in the helium. In addition, both cases show almost identical values to the gas-phase *B* constant, indicating that the rotations of the molecule are almost completely decoupled from the shell.

The renormalized *B* constant for CH_4 molecules of different intrinsic moments of inertia are summarized in Figure 6. The renormalized rotational constant of normal CH_4 is 5.10 cm^{-1} and for CD_4 is 2.48 cm^{-1}. These are in good agreement with the experimental nanodroplet values of approximately 5.0 and 2.5 cm^{-1}.[13,14,47,58] To put these small changes on a more convenient scale to display the effects of the mass of the probe, we have plotted the percentage increase in the renormalized *B* constant relative to the values of their gas-phase moments of inertia in Figure 6. Open circles correspond to results with full exchange and squares to their nonexchange counterparts. The effects of quantum statistics seem to be significant only for heavy probes (>12 × CH_4), with only very minor differences between the exchange and nonexchange results for lighter probes. This is consistent with what was observed for C_2H_2.[21]

To summarize the key results, the rotations of a light probe are largely decoupled from the helium shell, leading to almost no noticeable difference between the measured rotational constant and its intrinsic gas-phase value, regardless of whether the helium atoms are bosonic or not. In contrast, the rotations

of a heavy probe are more sensitive to the quantum statistics in the helium shell, resulting in a lighter effective moment of inertia when bosonic exchanges are operative. While this is true, the superfluidity of the shell seems to have no quantifiable relationship with the relative reduction in the B constant, with the superfluid fraction being close to unity for both light and heavy probes. These results suggest that the major determinant of how the B constant behaves in the case where the anisotropic interactions between the probe and the shell is weak is actually the intrinsic moment of inertia of the probe but not the superfluid fraction of the shell.

D. Incomplete Helium Shells. The next question is how much of a helium shell is necessary for the effects of quantum statistics to show up in the probe rotations. Experimentally, this question has been addressed by a number of authors,[16−19,25,59−62] who found that for OCS, CO, CO_2, HCCCN, and N_2O the renormalized rotational constant approaches the asymptotic droplet value in a nonmonotonic fashion. For OCS,[60] the initial decrease in the renormalized B constant undershoots the droplet value for a small number of ^{4}He atoms and then approaches the asymptotic value in an oscillatory fashion. Previous DMC results for the rotational excited state energy of SF_6[9,32] also show similar partial shell effects in which the renormalized B constant appears to have reached the asymptotic droplet value in a shell with only eight ^{4}He atoms. The situations are expected to be somewhat different between OCS and SF_6, because the helium−OCS interaction potential is highly anisotropic with the low-energy regions characterized by several rings of different sizes around the OCS molecular axis, while SF_6 is a spherical top molecule and the helium−SF_6 potential is more isotropic. For heavy probes like SF_6, the initial drop in B is consistent with the increase in moment of inertia caused by the rigid attachment of helium atoms to the low-energy regions on the rotor molecule. The first eight ^{4}He atoms seem to adiabatically follow the rotations of the SF_6. Beyond that, the renormalized B constant appears to reach its asymptotic droplet limit quickly, suggesting that further addition of ^{4}He does not result in any rigid attachment or additional rotational resistance.

Methane is another spherical top molecule, but its interaction with helium atoms is weaker than that of SF_6. Results for the renormalized B constants for 50 × CH_4 and 1 × CH_4 are shown in Figure 7 for $N = 1$ to 20 ^{4}He atoms with full exchange. For 50 × CH_4, the renormalized B constant seems to have reached the asymptotic limit at around $N = 6$. Beyond that, the effective B constant shows only minor variations up to 20 ^{4}He atoms. Clearly, the dominant effects of the ^{4}He shell on the rotations of the 50 × CH_4 are already present with a small number of ^{4}He atoms even before the completion of the first solvation shell. On first sight, this result seems to be similar to what was observed in SF_6. But in contrast to SF_6, the initial drop in B with the first few ^{4}He is *not* consistent with the rigid attachment of ^{4}He atoms, which would have led to a much more precipitous decrease in B indicated by the dotted line in Figure 7. Rather than following the molecule, the ^{4}He shell appears to be slipping relative to the rotations of the 50 × CH_4. After the addition of approximately six ^{4}He, the B constants appears to have reached its droplet limit, showing a roughly 15% decrease from its gas-phase value in agreement with Figure 6.

For the much lighter 1 × CH_4, the B constant decreases more slowly with the size of the ^{4}He cluster. The change in the effective B constant for 1 × CH_4 with number of ^{4}He atoms is shown in Figure 7b. The asymptotic droplet limit seems to be reached at around $N = 16$, but the absolute change in B in the droplet limit is only about 3% from its gas-phase value, which is consistent with Figure 6. By examining the ^{4}He radial density, we know that 16 ^{4}He corresponds approximately to the completion of the first solvation shell.

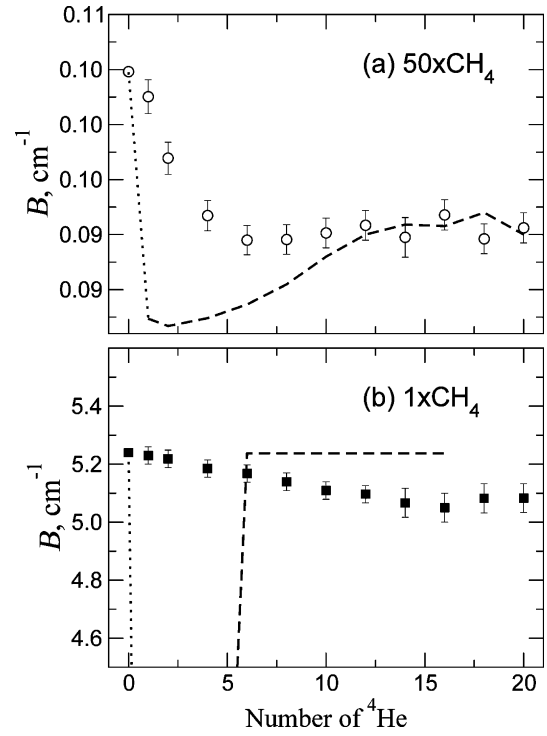

Figure 7. Effective B constant for (a) 50 × CH_4 and (b) 1 × CH_4 in clusters with different number of ^{4}He atoms, from 1 to 20. For 50 × CH_4, the renormalization of the B constant by the ^{4}He seems to reach the asymptotic limit at around six ^{4}He atoms, with only minor variations thereafter. For 1 × CH_4, the change in B with the number of ^{4}He atoms is much more gradual. The dotted line in each panel indicates the expected drop in B if the first ^{4}He were to follow the rotations of the CH_4 adiabatically. The dashed line in each panel indicates the expected B constant if the first-shell nonsuperfluid densities were to follow the rotation of the molecule adiabatically.

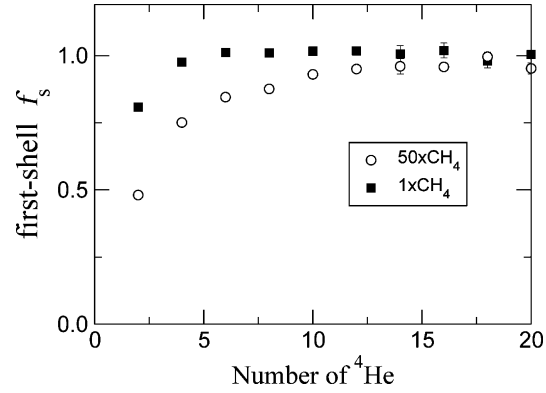

Figure 8. First-shell superfluid fractions for 50 × and 1 × CH_4 as a function of cluster size.

The B constant data in Figure 7 suggest that the CH_4 molecule is slipping relative to the helium shell. But to what extent is this related to the superfluidity of the shell? To further assess the nature of the adiabatic following (or the lack of it here), we show in Figure 8 the local superfluid fraction integrated out to the end of the first shell at around 4.3 Å for the incomplete helium shells corresponding to the sizes in Figure 7. For the 50 × CH_4, the superfluid fraction reaches the asymptotic limit at around $N = 12$, whereas for 1 × CH_4, the asymptotic limit

is already reached at $N = 6$. (This is the reverse of the asymptotic trends seen in Figure 7.)

To obtain a more quantitative estimate of the contribution of the superfluid activities to the slipping of the CH_4, we computed what the B constant should have been if the entire nonsuperfluid part of the helium shell was following the rotating probe adiabatically. The results are shown in Figure 7 as the dashed lines. These values were calculated using the superfluid fractions from Figure 8, assuming that the nonsuperfluid densities were rigidly attached to the rotor, with the mass of the nonsuperfluid helium distributed uniformly on a spherical shell (this is reasonable given the high symmetry of the CH_4 molecule, its weak anisotropic interactions with the heliums, and the angularly uniform helium densities observed in Figure 3) of radius 4.05 Å, which is the average distance of the heliums from the CH_4. For the $50 \times CH_4$, the dashed line somewhat overestimates the renormalization in the B constant for small clusters. They approach the asymptotic limit at around $N = 12$, and at that point start to coincide with the full PIMC results. This indicates that whereas the renormalization of the B constant seems to have reached the asymptotic limit at $N = 6$, the molecule is actually slipping more than the local superfluid fraction suggests. On the other hand, the difference is much more pronounced for the $1 \times CH_4$, where for $N < 6$ the dashed line severely underestimates the slipping of the rotor, indicating that the superfluidity the helium shell is responsible for a very tiny part of the slipping of the $1 \times CH_4$ relative to the shell. For $N \geq 6$ in $1 \times CH_4$, the first shell superfluid fraction from Figure 8 is not statistically precise enough to yield accurate estimates for B (a 0.001 difference in first shell f_s would produce a factor of 2 difference in the calculated B). For $N \geq 6$, the dashed line simply shows the $f_s = 1.0$ prediction, equal to the free gas-phase B value.

IV. Discussion

The results above point to a somewhat puzzling conclusion: modifying the moment of inertia of the probe alone changes the response of the ^{4}He shell and the renormalization in the B constant in a significant way when everything else, including the helium-rotor interaction potential, is held fixed. This implies that the renormalization in the B constant is not an indicative measure of the superfluid activities of the ^{4}He shell, as it is commonly assumed in the interpretations of droplet experiments. In order to understand the B constant renormalization correctly, the nature and the intrinsic properties of the probe must be treated as an integral part of the system.

The reason why the moment of inertia of the probe plays an important role in determining the superfluid response of the ^{4}He shell and its countereffects on the effective B constant can be understood qualitatively in the following way. First, consider a very heavy probe molecule. From the point of view of the ^{4}He atoms, a very heavy rotor appears static; therefore, the ^{4}He atoms are essentially experiencing an anisotropic potential that is rotating very slowing in space. Depending on the strength of the interaction and its angular dependence, the first few ^{4}He atoms will tend to seek out lower-energy regions on the potential surface. If the interactions are sufficiently attractive, these initial ^{4}He atoms will be sequestered into these low-energy regions and are then expected to follow the probe molecule adiabatically when it rotates. Because these ^{4}He atoms stick to the probe, they can no longer be considered indistinguishable from the rest of the ^{4}He atoms in the droplet. This forms the basis of the two-fluid model proposed by Whaley et al.[9] But in the case of CH_4, this adiabatic separation of the sequestered ^{4}He atoms from the rest of the droplet is not entirely clean. That is, because of the weaker anisotropy in the He−CH_4 interactions, the first few ^{4}He atoms are not tightly sequestered and they tend to slip relative to the rotations of the probe. This is evident from the comparison between the incomplete shell data and the rigid-top prediction shown in Figure 7a. In contrast to ^{4}He−SF_6, which has a much stronger anisotropy,[63] the concept of adiabatic following is less useful for ^{4}He−CH_4. However, it does appear that once the first few ^{4}He atoms fill up the low-energy regions of the ^{4}He−CH_4 potential, the rest of the ^{4}He essentially offers no further rotational resistance to the probe, which is similar to what is seen in the SF_6 calculations[32] and what is assumed in the two-fluid model.

On the other hand, the superfluid fraction of the ^{4}He shell is only a weak function of the intrinsic moment of inertia of the probe, in contrast with the effects observed in the renormalization of the B constant. While the B constant changes by a factor of 13% from its gas-phase value in $50 \times CH_4$, the superfluid fraction is close to unity. Therefore, the direct relationship between the superfluid activities of the ^{4}He shell and the renormalization in the B constant is difficult to quantify. This is further substantiated by the poor comparison between the B constant renormalization from the simulation data and the estimates based on the assumption that the nonsuperfluid part of the shell follows the rotations of the probe adiabatically. We also see that the ^{4}He shell density is strongly templated by the underlying anisotropy in the He−CH_4 potential when the probe is heavy, a fact that is consistent with the picture given above.

Turning to the light probes, it may seem surprising that according to Figure 3b the helium shell shows almost no awareness of the underlying $1 \times CH_4$, even though the He−CH_4 potential is just as strong in the case of $1 \times CH_4$ as for $50 \times CH_4$. This can be understood in terms of a "rotational smearing" effect, in which a very light rotor presents itself to the helium atoms as an almost spherical object because of rotational dispersion. The helium atoms see a $1 \times CH_4$ as an essentially spherical object, just like they would see an argon atom, for example (the interaction strength between He−Ar is actually very similar to that of He−CH_4[64]). In this case, the decoupling of the helium shell from the rotations of the probe is complete, as is evident from the discrepancies between the simulation data and the rigid-top predictions in Figure 7b, and the concept of adiabatic following is not applicable for very light probes. Consequently, the renormalization in the B constants bears no relationship at all with the superfluid activities of the helium shell, and the data in Figure 6 confirm that there is no difference between exchange and nonexchange heliums for light probes. An earlier DMC calculation for ^{4}He−SF_6 alluded to this rotational smearing effect,[9,32] but the results in this paper make this more clear due to the weaker anisotropy in the He−CH_4 interactions in comparison to He−SF_6.

Returning to the three factors we discussed earlier that should determine whether adiabatic following is in effect, we have seen clear indication in this system that the intrinsic moment of inertia of the CH_4 greatly affects the renormalization of B. Since we have kept the strength as well as the anisotropy of the interaction between CH_4 and helium fixed, the difference in B observed for heavy and light CH_4 in Figure 7 must be due to either the difference in the local superfluid density or the intrinsic dynamics of the CH_4. Figures 7 and 8 show that there is no clean separation between these two factors—changing the intrinsic moment of inertia of the molecule also affects the intensity of the local superfluidity which feeds back into the B

constant renormalization. It is also clear that the adiabatic following of the nonsuperfluid densities alone cannot fully explain the slipping of the rotating CH_4 relative to the helium shell. Figure 8 shows definitively that for light CH_4, the adiabatic following of the nonsuperfluid has almost nothing to do with the *B* constant renormalization. For heavy CH_4, the following of the nonsuperfluid part of the shell bears a more significant relationship to the renormalized *B* constant, but the slipping of the probe is still somewhat more than what the local superfluidity would suggest. These features are consistent with the general observations from the work of both Patel et al.[34] and Paolini et al.,[33] but it is clearly difficult to make a clean separation among the three factors and attribute the renormalization of the *B* constant to either local superfluidity or the intrinsic rotational dynamics of the probe or the anisotropy of the He−probe interactions alone. These three factors appear to be intricately correlated with each other.

Acknowledgment. This paper is based in part upon work supported by the National Science Foundation under Grant Numbers CHE-9970766 and CHE-0713981. The authors are grateful to Andrey Vilesov for the many helpful discussions on helium.

References and Notes

(1) Ceperley, D. M. *Rev. Mod. Phys.* **1995**, *67*, 279.
(2) Feynman, Richard P.; Hibbs, Albert R. *Quantum Mechanics and Path Integrals*; McGraw-Hill: New York, 1965.
(3) Tisza, L. *Nature* **1938**, *141*, 913.
(4) Landau, L. D. *J. Phys. USSR* **1941**, *5*, 71.
(5) Landau, L. D. *J. Phys. USSR* **1947**, *11*, 91.
(6) Andronikashvili, E. L. *J. Phys. USSR* **1946**, *10*, 201.
(7) Toennies, J. P.; Vilesov, A. F. *Annu. Rev. Phys. Chem.* **1998**, *49*, 1.
(8) Grebenev, S.; Toennies, J. P.; Vilesov, A. F. *Science* **1998**, *279*, 2083.
(9) Kwon, Y.; Huang, P.; Patel, M. V.; Blume, D.; Whaley, K. B. *J. Chem. Phys.* **2000**, *113*, 6469.
(10) Behrens, M.; Buck, U.; Frochtenicht, R.; Hartmann, M.; Huisken, F.; Rohmund, F. *J. Chem. Phys.* **1998**, *109*, 5914.
(11) Slipchenko, M. N.; Vilesov, A. F. *Chem. Phys. Lett.* **2005**, *412*, 176.
(12) Nauta, K.; Miller, R. E. *J. Chem. Phys.* **2001**, *115*, 8384.
(13) Skvortsov, Dmitry S.; Hoshina, Hiromichi; Sartakov, Boris G.; Vilesov, Andrey In *62nd International Symposium on Molecular Spectroscopy*; Miller, T. A., Eds.; The Ohio State University: Columbus, OH, 2007.
(14) Rudolph, S.; Wollny, G.; von Haeften, K.; Havenith, M. *J. Chem. Phys.* **2007**, *126*, 124318.
(15) Nauta, K.; Miller, R. E. *J. Chem. Phys.* **2000**, *113*, 9466.
(16) Tang, J.; Xu, Y. J.; McKellar, A. R. W.; Jager, W. *Science* **2002**, *297*, 2030.
(17) Tang, J.; McKellar, A. R. W. *J. Chem. Phys.* **2003**, *119*, 754.
(18) Xu, Y. J.; Jager, W.; Tang, J.; McKellar, A. R. W. *Phys. Rev. Lett.* **2003**, *91*, 163401.
(19) Tang, J.; McKellar, A. R. W.; Mezzacapo, E.; Moroni, S. *Phys. Rev. Lett.* **2004**, *92*, 145503.
(20) Paesani, F.; Whaley, K. B. *J. Chem. Phys.* **2004**, *121*, 5293.
(21) Zillich, R. E.; Paesani, F.; Kwon, Y.; Whaley, K. B. *J. Chem. Phys.* **2005**, *123*, 144301.
(22) Blinov, N.; Song, X. G.; Roy, P. N. *J. Chem. Phys.* **2004**, *120*, 5916.
(23) Blinov, N.; Roy, P. N. *J. Low Temp. Phys.* **2005**, *140*, 253.
(24) Miura, S. *J. Phys.: Condens. Matter* **2005**, *17*, S3259.
(25) Xu, Y. J.; Blinov, N.; Jager, W.; Roy, P. N. *J. Chem. Phys.* **2006**, *124*, 081101.
(26) Moroni, S.; Sarsa, A.; Fantoni, S.; Schmidt, K. E.; Baroni, S. *Phys. Rev. Lett.* **2003**, *90*, 143401.
(27) Zillich, R. E.; Whaley, K. B. *Phys. Rev. B* **2004**, *69*, 104517.
(28) Ramilowski, J. A.; Mikosz, A. A.; Farrelly, D.; Fajin, J. L. C.; Fernandez, B. *J. Phys. Chem. A* **2007**, *111*, 12275.
(29) Skrbic, T.; Moroni, S.; Baroni, S. *J. Phys. Chem. A* **2007**, *111*, 7640.
(30) Moroni, S.; Blinov, N.; Roy, P.-N. *J. Chem. Phys.* **2004**, *121*, 3577.
(31) Blume, D.; Mladenovic, M.; Lewerenz, M.; Whaley, K. B. *J. Chem. Phys.* **1999**, *110*, 5789.
(32) Lee, E.; Farrelly, D.; Whaley, K. B. *Phys. Rev. Lett.* **1999**, *83*, 3812.
(33) Paolini, S.; Fantoni, S.; Moroni, S.; Baroni, S. *J. Chem. Phys.* **2005**, *123*, 114306.
(34) Patel, M. V.; Viel, A.; Paesani, F.; Huang, P.; Whaley, K. B. *J. Chem. Phys.* **2003**, *118*, 5011.
(35) Trotter, H. F. *Proc. Am. Math. Soc.* **1959**, *10*, 545.
(36) Muser, M. H.; Berne, B. J. *Phys. Rev. Lett.* **1996**, *77*, 2638.
(37) Zare, R. N. *Angular Momentum*; Wiley: New York, 1988.
(38) Goldstein, H.; Poole, Charles; Safko, John *Classical Mechanics*; Addison Wesley: Reading, MA, 2002.
(39) Bander, M.; Itzykson, C. *Rev. Mod. Phys.* **1966**, *38*, 330.
(40) Norcliff, A. *J. Phys. A: Gen. Phys.* **1972**, *5*, 231.
(41) Cui, T.; Cheng, E.; Alder, B. J.; Whaley, K. B. *Phys. Rev. B* **1997**, *55*, 12253.
(42) Marx, D.; Muser, M. H. *J. Phys.: Condens. Matter* **1999**, *11*, R117.
(43) Mak, C. H.; Zakharov, S. *J. Phys. Chem. B* **2004**, *108*, 6760.
(44) Mak, C. H.; Zakharov, S.; Spry, D. B. *J. Chem. Phys.* **2005**, *122*, 104301.
(45) Metropolis, Nicholas; Rosenbluth, Arianna W.; Rosenbluth, Marshall N.; Teller, Augusta H. *J. Chem. Phys.* **1953**, *21*, 1087.
(46) Herzberg, Gerhard *Molecular Spectra and Molecular Structure*; Krieger Publishing Company: Malabar, FL, 1991.
(47) Nauta, K.; Miller, R. E. *Chem. Phys. Lett.* **2001**, *350*, 225.
(48) Buck, U.; Kohl, K. H.; Kohlhase, A.; Faubel, M.; Staemmler, V. *Mol. Phys.* **1985**, *55*, 1255.
(49) Aziz, R. A.; McCourt, F. R. W.; Wong, C. C. K. *Mol. Phys.* **1987**, *61*, 1487.
(50) Paesani, F.; Viel, A.; Gianturco, F. A.; Whaley, K. B. *Phys. Rev. Lett.* **2003**, *90*, 073401.
(51) Press, W. H.; Flannery, B. P.; Teukolsky, S. A.; Vetterling, W. T. *Numerical Recipes in C: The Art of Scientific Computing*; Cambidge Univercity Press: New York, 1995.
(52) Grebenev, S.; Hartmann, M.; Havenith, M.; Sartakov, B.; Toennies, J. P.; Vilesov, A. F. *J. Chem. Phys.* **2000**, *112*, 4485.
(53) Kwon, Y. K.; Whaley, K. B. *Phys. Rev. Lett.* **1999**, *83*, 4108.
(54) Paesani, F.; Zillich, R. E.; Kwon, Y.; Whaley, K. B. *J. Chem. Phys.* **2005**, *122*, 161106.
(55) Zilich, R. E.; Paesani, F.; Kwon, Y.; Whaley, K. B. *J. Chem. Phys.* **2005**, *123*, 114301.
(56) Paesani, F.; Kwon, Y.; Whaley, K. B. *Phys. Rev. Lett.* **2005**, *94*, 153401.
(57) Kwon, Y.; Raesani, F.; Whaley, K. B. *Phys. Rev. B* **2006**, *74*, 174522.
(58) The experimental data in ref 13 and unpublished data from Vilesov et al. contain two sets of measurements for CH_4 and CD_4. These two sets of data were obtained from two different analyses of the measured spectra. From the ground state data, the *B* constant renormalization in droplet helium is 4.4% and 4.0% for CH_4 and CD_4, respectively, whereas from the excited state data, they are 2.2% and 7.1%. These two sets of data are consistent in magnitude with the simulation results reported here.
(59) Topic, W.; Jager, W.; Blinov, N.; Roy, P. N.; Botti, M.; Moroni, S. *J. Chem. Phys.* **2006**, *125*, 144310.
(60) McKellar, A. R. W.; Xu, Y. J.; Jager, W. *J. Phys. Chem. A* **2007**, *111*, 7329.
(61) Surin, L. A.; Potapov, A. V.; Dumesh, B. S.; Schlemmer, S.; Xu, Y.; Raston, P. L.; Jager, W. *Phys. Rev. Lett.* **2008**, *101*, 233401.
(62) McKellar, A. R. W. *J. Chem. Phys.* **2008**, *128*, 044308.
(63) Pack, R. T.; Piper, E.; Pfeffer, G. A.; Toennies, J. P. *J. Chem. Phys.* **1984**, *80*, 4940.
(64) Maitland, Geoffrey C.; Rigby, Maurice; Smith, E. Brian *Intermolecular Forces*; Clarendon Press: Oxford, 1987.

JP900718D